JOURNAL OF CATALYSIS 149, 344–355 (1994)

# Vanadia–Titania Aerogels

## II. Spectroscopic Investigation of the Structural Properties

U. Scharf,* M. Schneider,† A. Baiker,† and A. Wokaun*·†

*Physical Chemistry II, University of Bayreuth, D-95440 Bayreuth, Germany, and †Department of Chemical Engineering and Industrial Chemistry, Swiss Federal Institute of Technology, ETH Zentrum, CH-8092 Zürich, Switzerland

Received February 22, 1994; revised June 1, 1994

**The structure of differently prepared vanadia–titania aerogels, with a nominal '$V_2O_5$' content varying between 5 and 30 wt%, has been characterized by Fourier transform infrared (FTIR) spectroscopy, laser Raman spectroscopy, secondary ion mass spectroscopy, $^{51}V$ nuclear magnetic resonance, and electron microscopy. Preparation parameters varied include the type of vanadyl alkoxide precursor, the sol–gel and calcination temperatures, and the heating rate used in supercritical drying. Common to all samples are the absence of long-range order and the presence of vanadia in highly dispersed form. The vanadia component was found to be mostly amorphous, whereas for the titania matrix small crystalline domains of anatase were detected. Up to a '$V_2O_5$' content of 20 wt%, no vanadyl vibrations were detected by Raman spectroscopy; in the FTIR spectra, bands due to an aggregated vanadyl species have been observed. At a '$V_2O_5$' content of 30 wt%, the presence of both two-dimensionally connected vanadia species and three-dimensional aggregates was deduced from the Raman spectra. Increasing the sol–gel reaction temperature accelerated the growth of vanadia clusters. Variation of the heating rate applied in the supercritical drying process resulted in cluster aggregation at the highest rate (120 K/h). The calcination temperature has a profound influence on the structure of mixed oxides: cluster formation and surface segregation of the vanadia were observed for calcination temperatures of 623–673 K; a more rigorous calcination treatment at 723 K induced the formation of three-dimensional $V_2O_5$ crystallites.** 

## INTRODUCTION

The advent of sol–gel techniques (1, 2) has opened interesting possibilities for the structural and textural tailoring of mixed oxides. In Part I, we reported on the preparation and morphological properties of novel vanadia–titania aerogels which exhibit excellent activity for the selective catalytic reduction (SCR) of NO by $NH_3$ (3). Vanadia–titania aerogels with high accessibility of the active vanadia component were synthesized by a two-stage sol–gel procedure with subsequent high-temperature supercritical drying. The SCR reaction rate (referred to vanadia content) was found to be similar to that measured for multiply grafted vanadia-on-titania catalysts.

In this article, the structure of these aerogels is characterized by spectroscopic techniques. We use the potential of vibrational spectroscopy [Fourier transform infrared (FTIR) and laser Raman] and magnetic resonance spectroscopy [$^{51}V$ nuclear magnetic resonance (NMR)] to investigate the influence of vanadia content and preparation parameters on structural features of the mixed oxides that are hardly accessible by other techniques, such as diffraction methods. In addition, some information on local connectivities between the constituents is obtained from secondary ion mass spectroscopy (SIMS).

In contrast to gel-type vanadia–titania catalysts, the physical and chemical properties of *supported* vanadia layers have been the subject of thorough investigations. It was found that these properties are influenced by nature of the support, vanadia loading, method of deposition, and calcination treatment. Vibrational (4–12) and $^{51}V$ NMR (13–16) studies led to the result that the catalytically most active vanadia species on titania correspond to extended, two-dimensionally connected patches of $VO_x$. Interaction of these species with the titania support gives rise to a distorted square-pyramidal coordination sphere of the vanadia centers, as opposed to the octahedral coordination in three-dimensional crystallites or aggregates and the tetrahedral coordination of isolated vanadia centers. Due to their sensitivity to changes in the coordination sphere, FTIR spectroscopy, Raman spectroscopy, and $^{51}V$ NMR are powerful tools to discriminate between the various types of species. Our assignments are thus based on earlier results obtained with grafted vanadia/titania catalyst systems (11, 12).

## EXPERIMENTAL

*Catalyst preparation.* The procedure used to synthesize the aerogels is described in detail in Part I (3). In the standard sol–gel preparation [labeled V20*STA* in



0021-9517/94 $6.00

TABLE 1

Composition, Preparation Parameters, and Surface Areas of the Investigated Samples

| Vanadia content | | Label | BET surface area ($m^2 g^{-1}$) | XRD crystallinity[a] | Sol–gel temperature (K) | Heating rate ($K h^{-1}$) | Calcination temperature (K) |
|---|---|---|---|---|---|---|---|
| wt% | at.% | | | | | | |
| 20 | 18.0 | V20*STA* | 192 | A | 298 | 60 | 573 |
| 0 | 0.0 | V0 | 182 | A | 298 | 60 | 573 |
| 5 | 4.4 | V5 | 194 | A | 298 | 60 | 573 |
| 10 | 8.9 | V10 | 183 | A | 298 | 60 | 573 |
| 30 | 27.4 | V30 | 195 | A | 298 | 60 | 573 |
| 100 | 100 | V100 | 25 | S, V | 298 | 60 | 573 |
| 20 | 18.0 | V20*ViP* | 157 | A | 298 | 60 | 573 |
| 20 | 18.0 | V20*STA*623 | 202 | A | 298 | 60 | 623 |
| 20 | 18.0 | V20*STA*673 | 178 | A | 298 | 60 | 673 |
| 20 | 18.0 | V20*STA*723 | 42 | A, R, S | 298 | 60 | 723 |
| 20 | 18.0 | V20*SGT*273 | 173 | A | 273 | 60 | 573 |
| 20 | 18.0 | V20*SGT*323 | 191 | A | 323 | 60 | 573 |
| 20 | 18.0 | V20*HR*8 | 152 | A | 298 | 8 | 573 |
| 20 | 18.0 | V20*HR*30 | 196 | A | 298 | 30 | 573 |
| 20 | 18.0 | V20*HR*120 | 181 | A | 298 | 120 | 573 |

[a] A, anatase; R, rutile; S, shcherbinaite; V, $V_2O_4$.

agreement with the nomenclature introduced in (3)] a binary sol with a nominal content of 20 wt% '$V_2O_5$' was prepared at 298 K and heated to supercritical conditions (533 K) at the rate of 60 K/h in a hermetically closed autoclave. After pressure release, the gel was calcined at 573 K, as detailed in Ref. (3).

The samples investigated in this study are identified in Table 1, together with the labels used throughout the text. The following preparation parameters have been varied with respect to the standard procedure mentioned above:

1. Nominal vanadia content, as calculated from the amount of vanadyl tri-*n*-propoxide (VOTP) used in the preparation (symbol *Vnn*, where *nn* is the nominal weight fraction of '$V_2O_5$')
2. Alkoxide precursor, i.e., replacement of VOTP with vanadyl tri-isopropoxide (*ViP*)
3. Sol–gel temperature (SGT)
4. Heating rate (HR) in the autoclave used to reach supercritical conditions
5. Temperature of calcination in air (using portions of the standard aerogels)

*Spectroscopic measurements.* Diffuse reflectance IR measurements were recorded on an FTIR Instrument (Digilab, Model FTS 80) equipped with an "environmental chamber" placed into a diffuse reflectance accessory (Spectra-Tech). Samples were pretreated by heating to 473 K under a flow of dried oxygen to remove physisorbed water, and were subsequently cooled to 298 K prior to the measurements. The cell was purged with a small flow of oxygen during the experiment. Five hundred twelve scans were accumulated for each spectrum, at a resolution of 2 $cm^{-1}$.

Prior to Raman measurements, samples were dried at 393 K, transferred to 3-mm-diameter test tubes under argon, and sealed to prevent rehydration. Spectra were excited using the 530.8-nm line of a krypton ion laser (Coherent, Model Innova 300). Twenty milliwatts of power was focused onto a 0.1-mm-diameter spot on the sample. For detection a triple spectrograph combined with a cooled, intensified multichannel detection system was used, which has been described and characterized elsewhere (17). Resolution was set at 5–6 $cm^{-1}$. Typically, the integration time corresponded to 100 s, and 10 data sets have been coadded for each spectrum.

Positive secondary ion mass spectra were recorded in an UHV apparatus (Leybold) equipped with a high-pressure chamber ($p \leq 1$ MPa), a preparation chamber ($10^{-6}$–$10^{5}$ Pa), and an analysis chamber ($10^{-8}$ Pa). The sample was transferred between the positions on a heatable/coolable sample rod. In the SIMS experiments, samples were bombarded with primary argon ions of 5-keV energy from a noble gas ion source (Leybold, Model IQE 12/38, emitter current 10 mA). The argon ion beam was rastered over a 1 × 1-mm area on the sample at a rate of 100 Hz; the current measured at the sample amounted to 6 $\mu$A. Secondary ions were collected from the central area of the sputter crater, 0.7 × 0.7 mm in size; spectra were registered in the range 1–200 amu with a quadrupole mass spectrometer (Leybold, Model SSM 200, resolution of 0.7 amu) (18).

Scanning electron micrographs were recorded on a JEOL instrument (Model JSM-840 A) with a 20-keV electron beam.

$^{51}V$ NMR measurements were performed on a high-resolution solid-state NMR spectrometer (Bruker, Model MSL 300). Static $^{51}V$ spectra were recorded on a wide-line probe head. The length of a nonselective $\pi/2$ pulse was adjusted with a liquid $VOCl_3$ reference sample, as described in Ref. (16). With the catalyst samples, the carrier frequency was adjusted to the central $(-\frac{1}{2} \leftrightarrow \frac{1}{2})$ transition of the $I = 7/2$ nucleus, which is influenced by the quadrupolar interaction only in second order. To realize a selective $\pi/2$ pulse on the central transition, the length of the nonselective pulse was reduced (14) by a factor of $I + \frac{1}{2} = 4$ to a value of 1 $\mu$s. A recycle delay of 700 ms has been used. The number of accumulated scans varied between 300 and 20,000, depending on the vanadia content of the sample. Chemical shifts are referred to $VOCl_3$ used as an external standard.

## RESULTS

### *Influence of Vanadia Content*

*FTIR investigations.* Vibrational spectra of vanadia–titania aerogels containing different fractions of vanadia (between 5 and 30 wt% nominal '$V_2O_5$', sample series V5–V30) provide clear evidence that a chemical reaction is taking place during preparation when the vanadyl tri-*n*-propoxide precursor is added to the redispersed $TiO_2$ matrix. FTIR spectra in the hydroxyl stretching region (Fig. 1a) are presented first. The spectrum of the $TiO_2$ aerogel is characterized by a composite band (bottom trace). The maxima of the double peak above 3700 $cm^{-1}$ are located at 3725 and 3714 $cm^{-1}$. Below 3700 $cm^{-1}$, a peak at 3688 $cm^{-1}$ with shoulders at 3675 and 3640 $cm^{-1}$ is seen. These hydroxyl stretching vibrations are known from the spectrum of anatase, and have been assigned to basic and acidic surface OH groups (19).

Addition of 5 wt% '$V_2O_5$' causes a drastic decrease in the titania vibrations above 3700 $cm^{-1}$, which are assigned to basic hydroxyl groups. The peak at 3688 $cm^{-1}$, which is the most intense with titania, has changed into a small shoulder. Maximum absorption is now found at 3670 $cm^{-1}$. For a '$V_2O_5$' content of 10 wt% in the aerogel, the trend of the changes described continues, with a red shift of the maximum to 3665 $cm^{-1}$. In the spectrum of the catalyst containing 20 wt% '$V_2O_5$, a band at 3655 $cm^{-1}$ is observed, which is assigned (20, 21) to the $\nu$(V–OH) stretching vibration. The signature of the titania hydroxyl groups remains visible on the low-frequency edge of this band. With the 30 wt% '$V_2O_5$'–$TiO_2$ sample (V30), the maximum is found at 3650 $cm^{-1}$; titania hydroxyl absorptions have become minor. The vanadia aerogel (V100) does not exhibit bands in this spectral region (top trace).

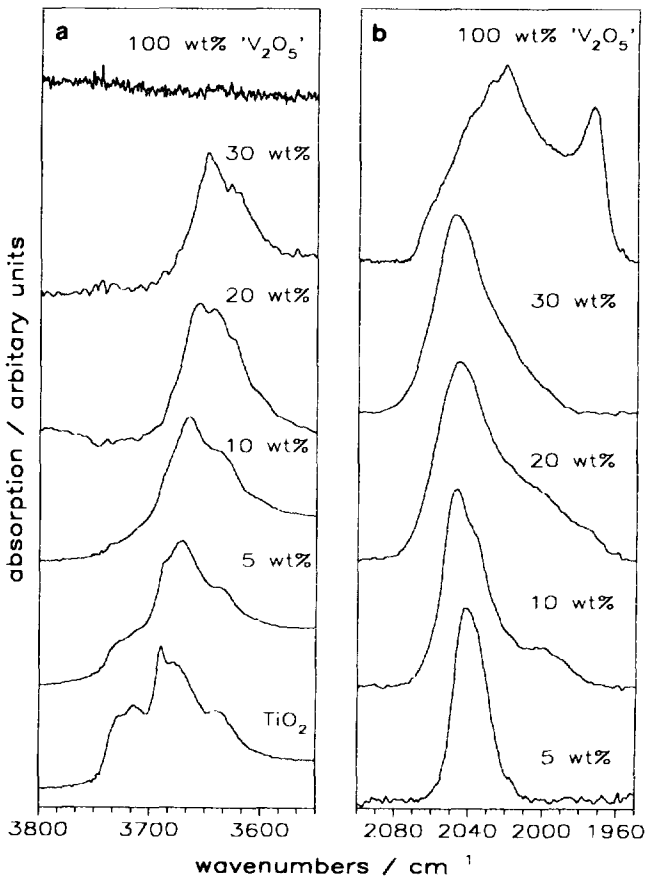


FIG. 1. FTIR spectra of aerogels with different vanadia contents, as indicated in the figure (in wt% '$V_2O_5$,' samples V0–V100). (a) OH stretching region; (b) $\nu$ (V=O) overtone region (see text). Diffuse reflectivity spectra $I_r/I_0$ were recorded as described under Experimental and are presented as normalized "pseudoabsorbance" spectra $\{-\log I_r/I_0\}$.

Next we focus on the vanadyl (V=O) stretching vibration. As the fundamental in the 1000 $cm^{-1}$ region is obscured by intense skeletal absorptions of the titania around 980 $cm^{-1}$, observation of the overtone region around 2000 $cm^{-1}$ turned out to be more informative (Fig. 1b). A vanadia absorption around 2042 $cm^{-1}$ is detected for all catalysts; with higher loadings the maximum shifts to 2047 $cm^{-1}$. This band is assigned to vanadia centers in a square-pyramidal coordination sphere of oxygen ligands, as known from supported catalysts (22–24); a shift to higher wavenumbers indicates a stronger interaction with the titania matrix. In the spectrum of the 10 wt% '$V_2O_5$' catalyst, a shoulder at 2038 $cm^{-1}$ is observed, which decreases with increasing vanadia content. At the same time, the band is broadened toward lower wavenumbers, indicating the presence of $VO_x$ species which interact less strongly with the titania matrix. The pure vanadia aerogel (V100) shows a double peak with maxima at 2020 and 1970 $cm^{-1}$, indicating the predominance of three-

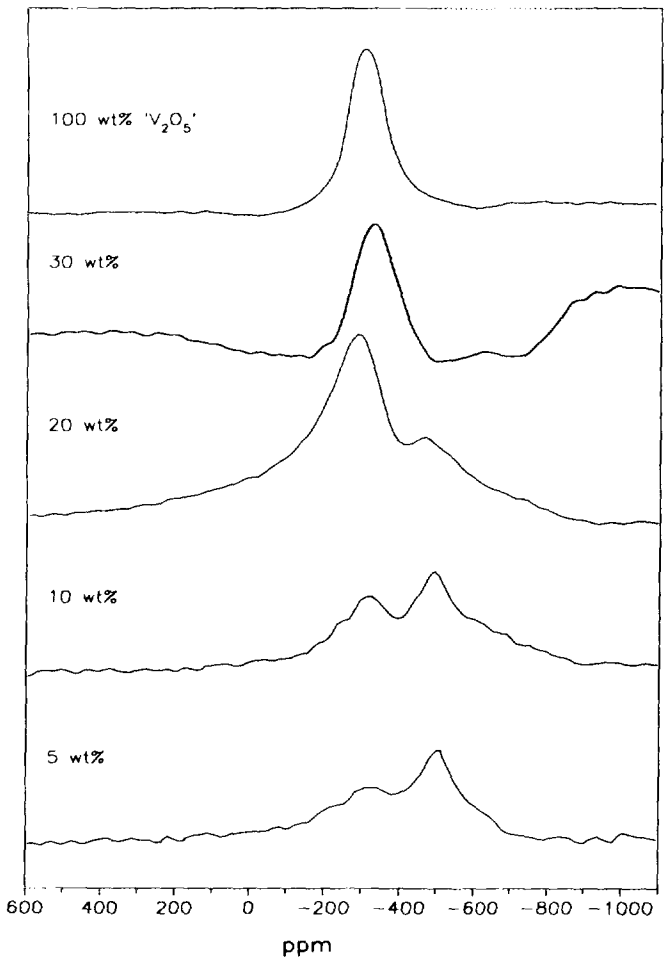


FIG. 2. Normalized $^{51}V$ NMR spectra of aerogels with different vanadia contents (wt% '$V_2O_5$,' samples V5–V100). Parameters of the experiment are indicated under Experimental.

dimensional $V_2O_5$ aggregates. The feature at 2047 $cm^{-1}$ mentioned above is still visible as a shoulder.

*$^{51}V$ NMR spectra.* Changes in coordination of the vanadia component are evident in the $^{51}V$ NMR spectra (Fig. 2). At a '$V_2O_5$' content of 5 wt%, the signal at approximately −490 ppm due to tetrahedrally coordinated vanadia centers (14, 25) is dominant. The presence of octahedrally coordinated species is indicated by a weaker shoulder at approximately −290 ppm (16, 25). An increase in '$V_2O_5$' content to 10 wt% leads to a clearly resolved peak at approximately −290 ppm; its intensity is still smaller than that of vanadia in tetrahedral coordination. In contrast, for the vanadia–titania aerogel with 20 wt% '$V_2O_5$' (V20*STA*), this relation is reversed, with the octahedrally coordinated vanadia species dominating in intensity and the tetrahedral vanadia representing a minority species. The 30 wt% sample (V30) gives rise to a spectrum practically identical to that of pure $V_2O_5$ (top trace in Fig. 2) and is typical of octahedrally coordinated vanadia.

*Laser raman investigations.* Raman spectra of these catalysts in the region 250–1100 $cm^{-1}$ are presented in Fig. 3. The equally prepared $TiO_2$ aerogel (bottom trace) shows the typical Raman vibrations of anatase at ≈400, ≈515, and ≈635 $cm^{-1}$. The inelastic scattering by the amorphous gel gives rise to an intense, broad, and unstructured background. On addition of vanadia a broad band appears between 470 and 400 $cm^{-1}$, which is attributed to a superposition of various small vanadia clusters (26, 27). Anatase vibrations are still clearly distinguishable as the narrower bands at ≈400 and 515 $cm^{-1}$.

In the spectrum of the binary aerogel with 10 wt% '$V_2O_5$' (V10), the broad band centered around 450 $cm^{-1}$ has increased in intensity and merges with the anatase vibrations at 512 and 400 $cm^{-1}$. The titania vibration at 635 $cm^{-1}$ also appears to be broadened. A weak and broad

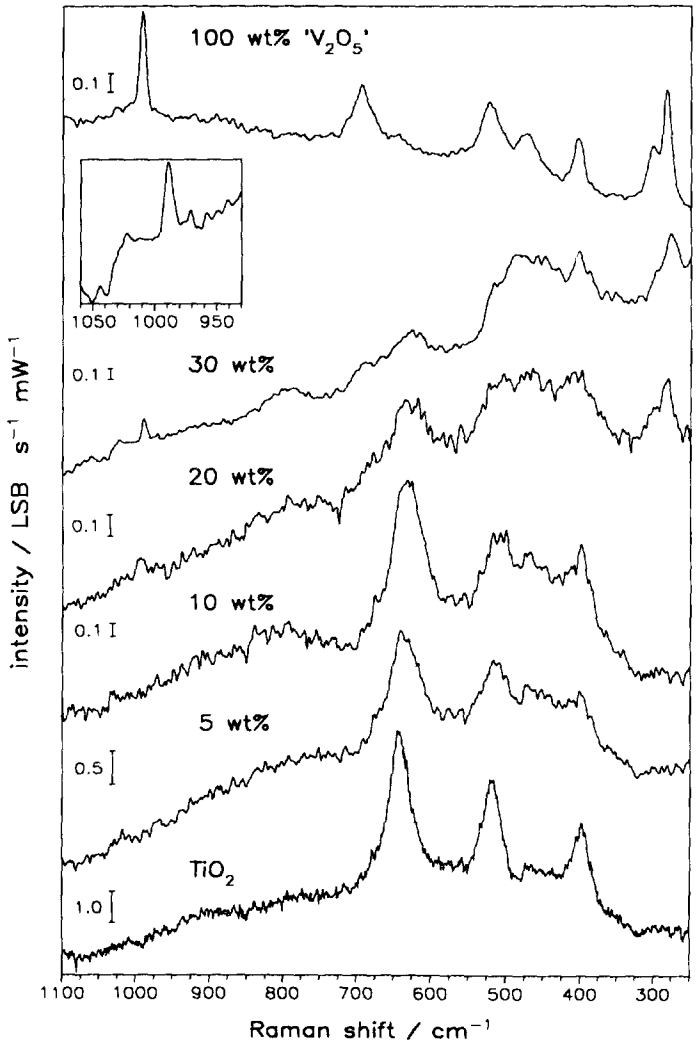


FIG. 3. Raman spectra of aerogels with different vanadia contents (wt% '$V_2O_5$,' samples V0–V100). Spectral acquisition parameters are indicated under Experimental. For the sample containing 30 wt% '$V_2O_5$,' the region 950–1050 $cm^{-1}$ is shown on an expanded vertical scale.

band at ≈700–820 $cm^{-1}$, assigned to the asymmetric O–V stretching modes of di- and trimeric vanadates (26, 27), is best seen in the spectrum of the V10 sample. For higher vanadia contents, this band decreases again, indicating that the number of small clusters decreases in favor of larger structures.

For a '$V_2O_5$' content of 20 wt% a new band appears in the Raman spectrum at 284 $cm^{-1}$. This vibration is assigned to the deformational motion δ (V=O) of multilayered $VO_x$, and has been described for $V_2O_5$ (28). In the spectrum of sample V20, the anatase vibrations completely overlap with a variety of stretching and deformational modes of small vanadia clusters. The latter assignment is based on Raman studies of various vanadates in solution (26, 27).

In the spectrum of V30 (30 wt% '$V_2O_5$'), a narrow band at 996 $cm^{-1}$ has developed, which is due to the ν (V=O) stretching vibration in multilayer structures as found in crystalline $V_2O_5$. The presence of three-dimensional vanadia domains or aggregates is confirmed by the observation of the matching vibrational modes of crystalline $V_2O_5$ in the low-frequency region (28), as may be seen by comparison with the spectrum of the vanadia aerogel (top trace). In addition, a weak, broad band at ≈1020 $cm^{-1}$ is detected for V30, as shown on an expanded scale in the inset to Fig. 3. This characteristic band is assigned (29–31) to extended two-dimensionally connected patches of vanadia which are well spread on titania surfaces. The appearance of this structural feature was accompanied by a distinct increase in SCR activity, as emerges from a comparison with the activity data shown in Part I (3).

The vanadia aerogel (V100) consists of crystalline $V_2O_5$ domains that are clearly identified by the Raman bands at 992 $cm^{-1}$ {ν(V=O)}, 695 $cm^{-1}$ {$\nu_{as}(V_3O)$}, 523 $cm^{-1}$ {$\nu_s(V_3O)$}, 472 $cm^{-1}$ {δ($V_2O$)}, 401 $cm^{-1}$ {δ(VO)}, 299 $cm^{-1}$ {δ($V_3O$)}, and 280 $cm^{-1}$ {δ(V=O)} (27, 28). A strong inelastic scattering background indicates the presence of an amorphous matrix. Similarly, the observed broadening of the peaks, as compared with spectra of highly crystalline samples, suggests that the vanadia is partly amorphous, as reported for xerogels by Sanchez *et al.* (31).

*SIMS spectra.* To probe vanadia–titania connectivities, i.e., the presence of V–O–Ti bridges, positive SIMS spectra have been recorded (Fig. 4). The spectra of the $TiO_2$ aerogel (V0, bottom) and of the vanadia aerogel (V100, top) are included for reference. Titania-related fragment ions ($Ti^+$, $TiO^+$, $TiO_2^+$, $Ti_2^+$, $Ti_2O^+$, and $Ti_2O_2^+$) are identified by verifying the appropriate ratios of the *five* titanium isotopes; similarly, the $V^+$ and $VO^+$ ion signals show the signature of the *two* vanadia isotopes. The intensities of the signals that correspond to the relevant isotopic combinations (cf. Fig. 4) agree well with the ratios expected from the relative isotopic abundances.

With the sample containing 5 wt% '$V_2O_5$' (spectrum not shown), the peaks at $m/z$ = 51 and 52 which correspond to the two isotopes of vanadium can be identified on the high-mass side of the $Ti^+$ peaks. Informative additional mass peaks appear at $m/z$ = 99, 115 (weak), and 131; they are assigned to the elementally mixed fragments $TiV^+$, $TiVO^+$, and $TiVO_2^+$. No signals due to fragments containing two vanadium atoms were detected in this spectrum. These fragments do, however, appear at $m/z$ = 102 ($V_2^+$), 118 ($V_2O^+$), and 134 ($V_2O_2^+$) if the '$V_2O_5$' fraction is increased to 10 wt% (sample V10, second trace from bottom in Fig. 4). The latter peaks further grow in intensity as the '$V_2O_5$' content is increased to 20 and 30 wt%.

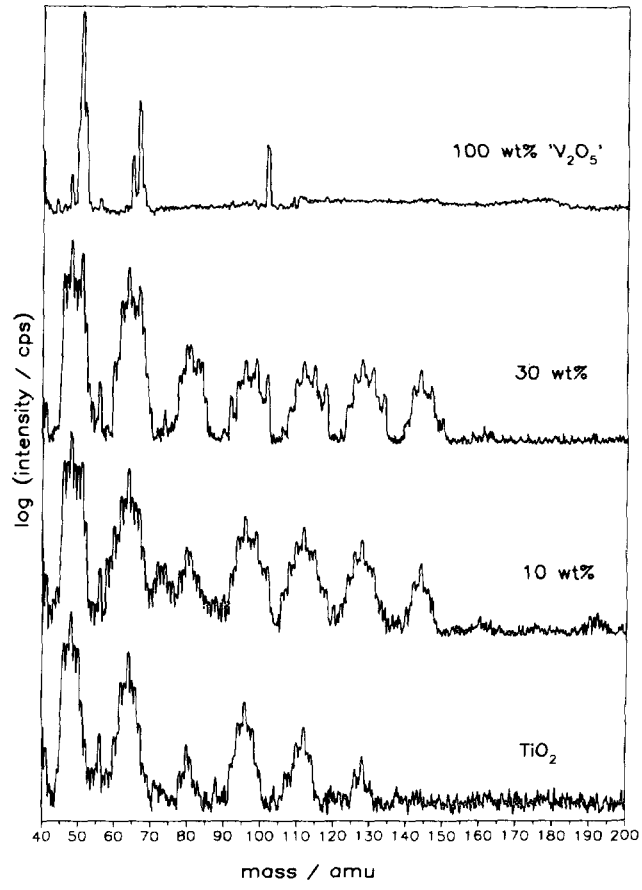


FIG. 4. SIMS spectra of titania (sample V0, bottom) and vanadia (sample V100, top) aerogels, as well as of vanadia–titania aerogels V10 and V30 containing 10 and 30 wt% '$V_2O_5$,' respectively. Groups of lines are due to the various isotopic combinations of V and Ti in the homo- and heteroelemental clusters, as described in the text.

Changes in the relative intensities of the different fragments ions are presented in graphic form in Fig. 5. The mass peaks have been assembled into three groups containing two metal atoms and zero, one, or two oxygen atoms, respectively. Within each group of three species, the sum of intensities of all possible isotope combinations was set equal to 100%. Relative intensities of the three elemental combinations (i.e., $Ti_2O_n^+$, $TiVO_n^+$, and $V_2O_n^+$,

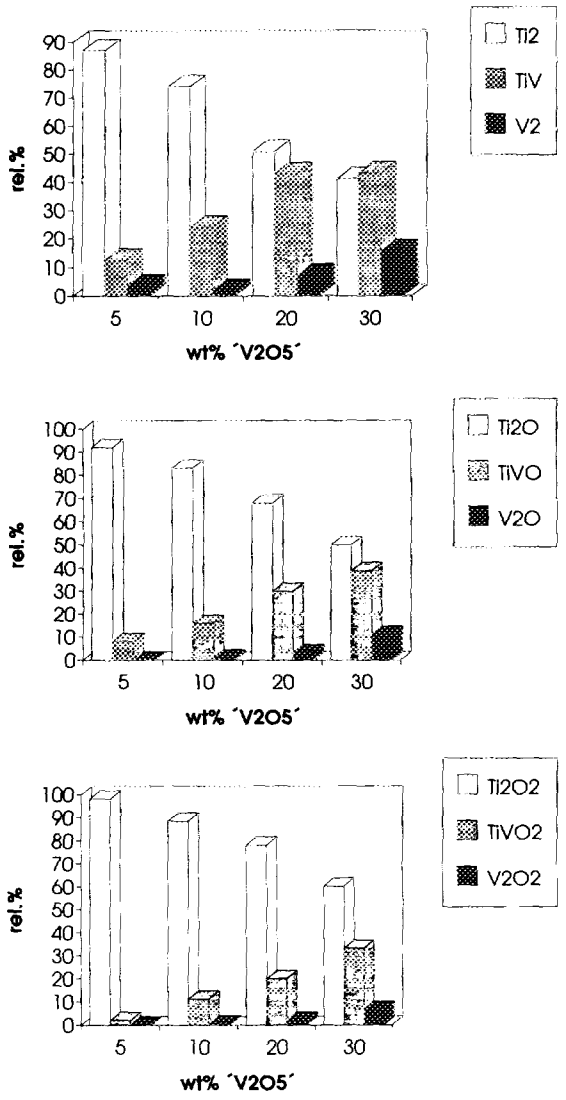


FIG. 5. Relative intensities of homo- and heteroelemental cluster fragments. White, gray, and shaded bars correspond to $Ti_2O_n$, $TiVO_n$, and $V_2O_n$, respectively. Three groups of fragments are analyzed containing $n$ = 0 (top), 1 (middle), and 2 (bottom) oxygen atoms. The abscissa in each graph is the '$V_2O_5$' content of the aerogel (in wt%). (*Note.* $Ti_2O_0$ is identical with $Ti_2$.)

$n$ = 0, 1, or 2) have been calculated, as shown in the bar graphs of Fig. 5. These results are discussed below.

*Scanning electron microscopy (SEM).* Scanning electron micrographs (Fig. 6) show an unstructured, spongelike appearance for the $TiO_2$ aerogel and for the samples with low vanadia contents (5 and 10 wt% '$V_2O_5$'). Catalysts with a higher vanadia fraction (right-hand side of Fig. 6) appear to consist of more densely packed aggregates, resembling reaction-limited aggregates of spheres, with a less open surface. This morphology is fully developed in the $V_2O_5$ aerogel: Small spheres are aggregated to form patches, which in turn assemble into larger spheres, with a typical fractal appearance.

*Influence of Vanadia Alkoxide Precursor*

When vanadyl tri-isopropoxide is used as the alkoxide precursor instead of vanadyl tri-*n*-propoxide, a gel with distinctly different structural and morphological properties resulted [sample V20 *ViP*, cf. (3)]. The Raman spectrum of this catalyst (not shown) is characterized by two broad bands centered at 460 and 800 $cm^{-1}$ which are attributed to small, defined vanadia clusters.

*Influence of Calcination Temperature*

To isolate the influence of selected sol–gel preparation parameters, a constant composition of the aerogels (20 wt% '$V_2O_5$', 80 wt% '$TiO_2$', V20*STA*) was selected. Results obtained on varying the calcination temperature are presented in Figs. 7 and 8. The Raman spectrum taken after calcination at 573 K (bottom trace) is the same as in Fig. 3, and is used as a reference for discussing the influence of the parameter variations. This spectrum is characterized by anatase vibrations at 400, 512, and 634 $cm^{-1}$, which are broadened by unresolved vanadia modes between 300 and 600 $cm^{-1}$. A peak at 286 $cm^{-1}$ assigned to $\delta$ (V=O) (27, 28) indicates the formation of three-dimensional vanadia agglomerates.

Calcination at 623 and 673 K (samples V20*STA*623, V20*STA*673) gives rise to structurally similar aerogels, as indicated by their Raman spectra (Fig. 7). The latter are dominated by a broad band with a maximum at ≈465 $cm^{-1}$ and a weaker band around 800 $cm^{-1}$, which are assigned to symmetric and asymmetric stretching vibrations of various small vanadia clusters (up to tetrameric species) (26, 27). Apparently vanadia species are accumulating and spreading on the surface of the aerogels. Consequently, the vibrational modes of the titania are weakened and are no longer observed as resolved bands. The top spectrum was recorded on a sample calcined at 723 K. From the prominent bands at 996, ≈700, 526, and 286 $cm^{-1}$ it emerges that the vanadia fraction contains crystalline $V_2O_5$ (28), as evidenced independently by X-ray analysis in Part I (3). The anatase fraction of the titania gives rise to weak shoulders at 625 and 512 $cm^{-1}$. In view of the modest signal-to-noise ratio, the Raman bands expected for the rutile fraction of this sample, at 612 and 440 $cm^{-1}$, are not discernible due to the lower scattering cross section of this modification.

The SIMS spectra of these differently calcined catalysts have been quantified in the same way as described above for Fig. 5. Equal trends are seen in Fig. 8 within each of the three groups of fragment ions. The fraction of agglomerated vanadia, which results in fragments containing two vanadium atoms, increases with calcination temperature, in complete accordance with the Raman spectroscopic observations. The $V_2O_5$ fraction is minor after calcination at 573 K and increases with the samples calcined at 623

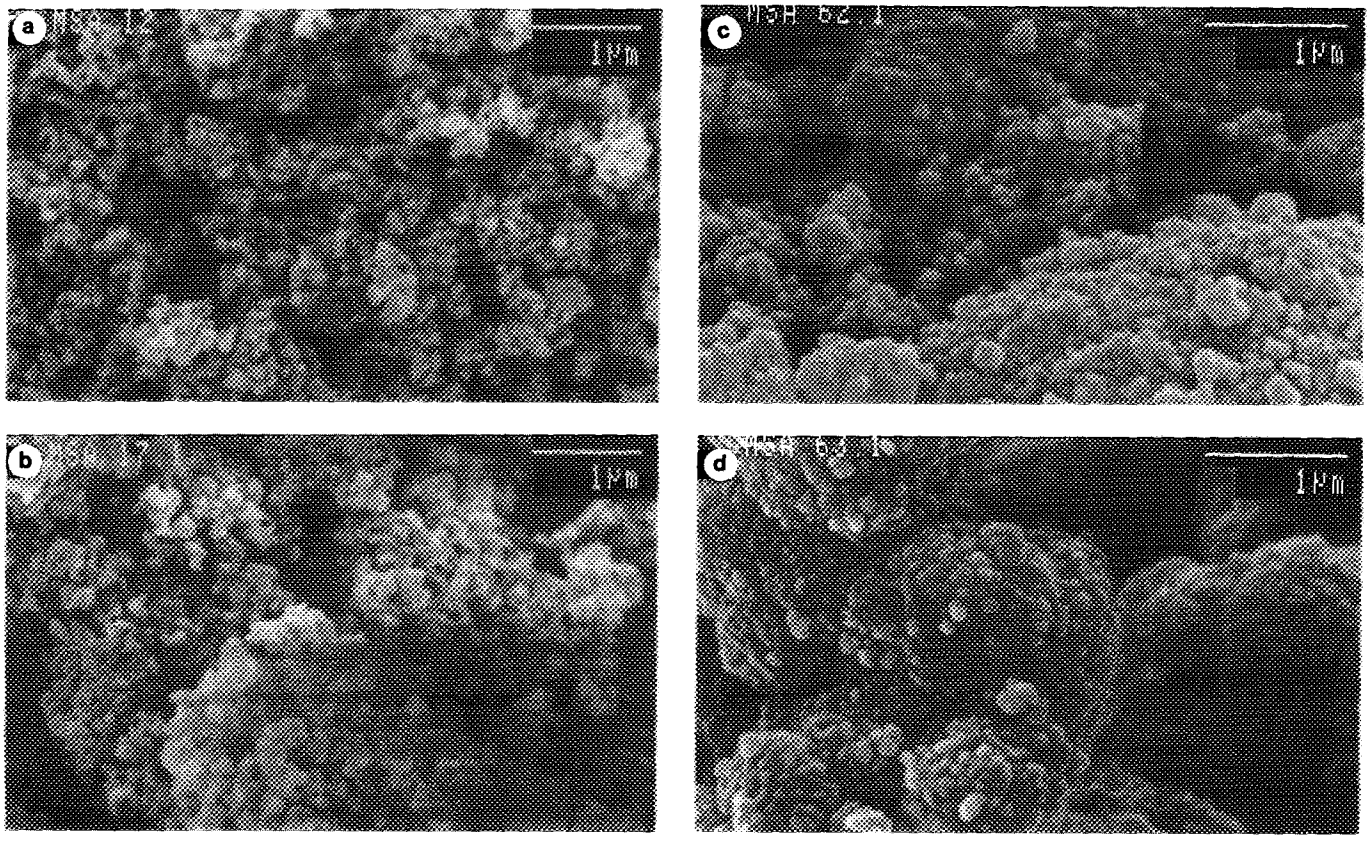


FIG. 6. Scanning electron micrographs of aerogels, showing the influence of vanadia content: (A) V0, titania; (B) V10, 10 wt% '$V_2O_5$'; (C) V30, 30 wt% '$V_2O_5$'; (D) V100, vanadia aerogel.

or 673 K. The aerogel calcined at 723 K exhibits a drastic increase in the contribution of fragments $V_2^+$, $V_2O^+$, and $V_2O_2^+$. The fraction of mixed fragments (containing one nucleus each of V and Ti) remains nearly unchanged on variation of the calcination temperature. The homonuclear titania cluster ions do not show significant changes either.

*Influence of Heating Rate*

Variation of the heating rate employed for reaching supercritical conditions did not lead to significant structural changes in the resulting aerogels. The Raman spectra (Fig. 9) of the aerogels supercritically dried at heating rates of ≈8, 30, and 60 K/h are nearly equal within experimental accuracy. Besides the three characteristic anatase vibrations, the presence of three-dimensionally aggregated vanadia is apparent from the observation of a δ(V=O) vibration at ≈280 $cm^{-1}$. Stretching vibrations of these $VO_x$ species cause the observed broadening of the titania vibrations at 400, 512, and 628 $cm^{-1}$. The highest heating rate employed, i.e., 120 K/h (sample V20*HR*120), results in broad bands with maxima at ≈460 and ≈800 $cm^{-1}$. This pair of frequencies is again assigned to the symmetric and asymmetric stretching vibrations of small vanadia clusters. The weak band around 635 $cm^{-1}$ arises from crystalline particles of anatase.

*Influence of Sol–Gel Temperature*

The influence of sol–gel temperature is shown in Fig. 10. A reaction temperature of 273 K (V20*SGT*273, bottom trace) results in a spectrum similar to that recorded for the standard preparation temperature of 298 K (V20*STA*, middle trace). Observation of a δ(V=O) vibration (286 $cm^{-1}$) and the broadening of the titania vibrations around 460 and 800 $cm^{-1}$ indicates that $VO_x$ particles of ill-defined structure are adhering to the surface of the $TiO_2$ matrix.

A sol–gel temperature of 323 K leads to the buildup of small clusters at the surface (top trace of Fig. 10). Only weak traces of the titania vibrations remain visible, which indicates that the $TiO_2$ component has been largely covered by vanadia. FTIR spectra of the OH stretching region (not shown) indicate that the mixing temperature does not alter the extent of reaction between the vanadyl alkoxide and the basic OH groups of the titania matrix. The three spectra obtained for samples V20*SGT*273, V20*STA*, and V20*SGT*323 are very similar in this spectral region.

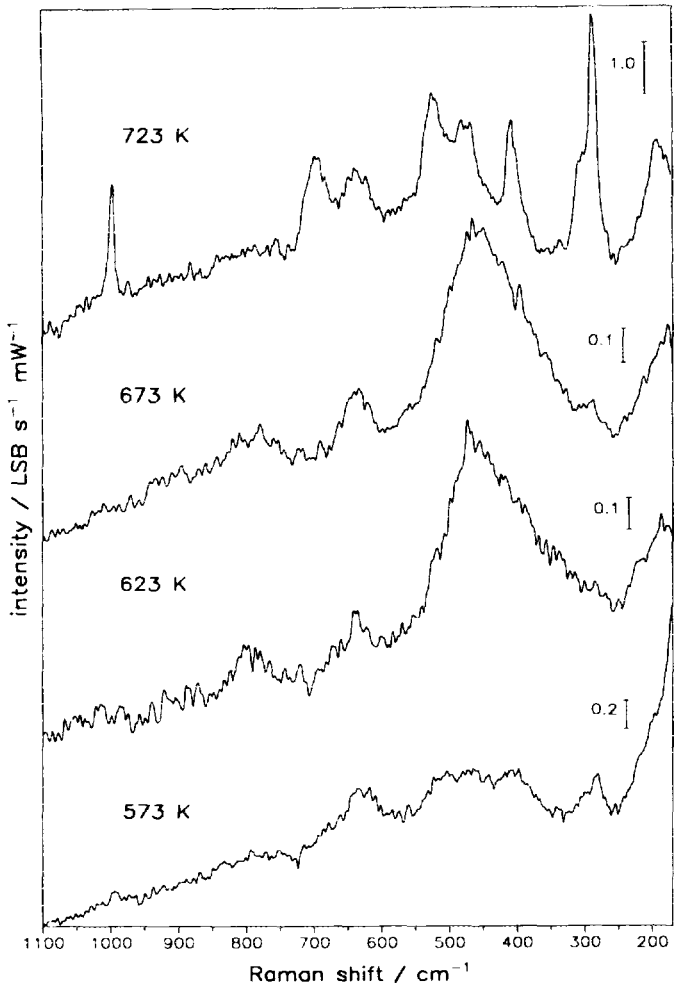


FIG. 7. Influence of calcination temperature on the Raman spectra of the V20*STA* series (20 wt% '$V_2O_5$') calcined at 573, 623, 673, and 723 K, respectively. Intensities in least significant bit (LSB) of the multichannel detector (17) have been normalized with respect to integration time and incident power.

Thus it appears that the chemical connectivity between the vanadyl species and the basic hydroxyl groups reaches "completion" at all of the reaction temperatures employed.

## DISCUSSION

FTIR spectra of the OH stretching region provide clear evidence for a chemical reaction between the two components: In the mixing step, the vanadyl alkoxide precursor attaches to the basic hydroxyl groups of the redispersed titania, in a reaction similar to the grafting of vanadia onto titania by the alkoxide–hexane route (23, 32, 33). Depletion of the corresponding IR signals reaches completion at a '$V_2O_5$' content of 10 wt%.

For low '$V_2O_5$' contents (up to 10 wt%), predominantly tetrahedral coordination of the vanadia centers has been deduced from $^{51}V$ NMR; these sites are capable of coordinating additional ligands. The development of various oligomeric vanadia clusters gives rise to broad and unstructured bands in the Raman spectra.

In an acidic medium, the acid-catalyzed hydrolysis of the vanadyl alkoxide precursor is expected (1) to proceed fast. For the present system, we note that the rate of condensation reactions with the basic Ti–OH groups of the redispersed titania appears to be higher than the *homo*condensation rate between hydrolyzed vanadium species.

At higher '$V_2O_5$' contents, the signals of small vanadia domains appear in the Raman spectra. For these higher concentrations of the hydrolyzed vanadyl alkoxide precursor, the more reactive, basic Ti–OH groups are rapidly depleted. Thereafter, the *homo*condensation reaction

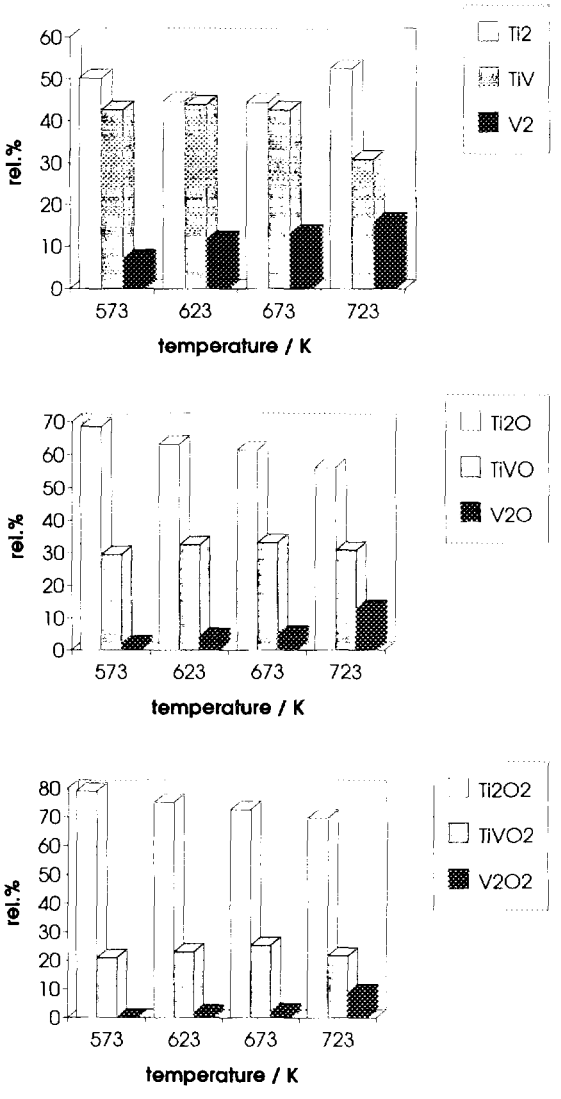


FIG. 8. Influence of calcination temperature (abscissa) on the relative intensities of homo- and heteroelemental fragment ions, recorded in the SIMS spectra of the V20*STA* series (20 wt% '$V_2O_5$') calcined at 573, 623, 673, and 723 K, respectively. Symbols are defined as in Fig. 5.

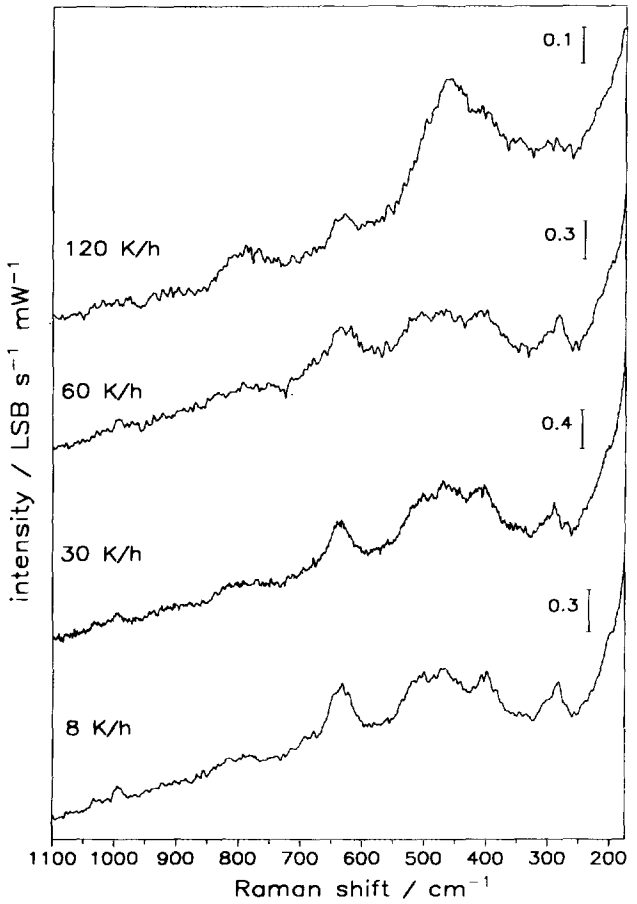


FIG. 9. Influence of the heating rate employed during supercritical drying on the Raman spectra of the vanadia–titania aerogels with 20 wt% '$V_2O_5$' (V20*HR* series).

(linking of adjacent V–OH groups) competes efficiently with anchoring at the remaining, acidic Ti–OH groups; in this process, vanadia clusters are formed and subsequently immobilized at the surface of the titania domains. At even higher vanadia contents, the vanadia clusters continue to grow, despite the fact that part of the titania surface is still uncovered. This development is evident both in the vibrational spectra and in the SIMS results, where a parallel increase in $V_2O_n^+$ and $VTiO_n^+$ fragments was observed. The existence of parts of the titania surface that remain uncovered by vanadia is evident from Raman, SIMS, and $NH_3$ adsorption experiments to be reported elsewhere.

Next we address the structure of the vanadia centers. Up to a '$V_2O_5$' content of 20 wt%, signals due to V=O stretching vibrations are detected only in the FTIR spectra; the corresponding Raman signals appear too weak to be observed. Interaction with the $TiO_2$ matrix appears to be stronger as compared with the supported catalyst systems; a similar trend has previously been observed for vanadia/silica xerogels (25). The shift of the FTIR-detected overtone to higher wavenumbers (Fig. 1b) suggests that the strength of interaction is increasing with vanadia content. At the highest '$V_2O_5$' fraction of 30 wt%, three-dimensional aggregates resembling crystalline $V_2O_5$ are detected. The titania skeletal vibrations are superimposed by the intense signals due to this species. The fraction of $Ti_2O_n^+$ fragments detected by SIMS is somewhat decreased but still very substantial, reflecting the bulk composition. At this stage, the homocondensation reactions between V–OH groups and/or heterocondensation of vanadium–oxo clusters leads to growth of the vanadia clusters, forming three-dimensional structures. In addition to the paracrystalline particles, the signature of two-dimensional layer structures is now evident from a weak signal at $\approx$1020 cm$^{-1}$ in the Raman spectrum (Fig. 3). In both types of species, the vanadia centers are characterized by fivefold (square-pyramidal) coordination with a distant sixth oxygen ligand.

This picture of changes in structure with increasing vanadia content is supported by the observations in the

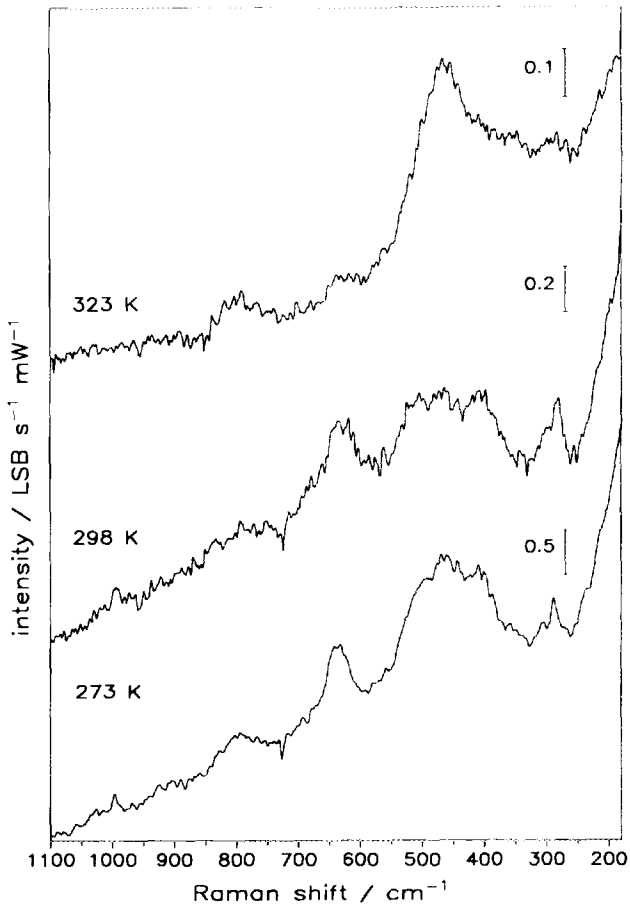


FIG. 10. Influence of the sol–gel reaction temperature on the Raman spectra of vanadia–titania aerogels with 20 wt% '$V_2O_5$' (V20*SGT* series).

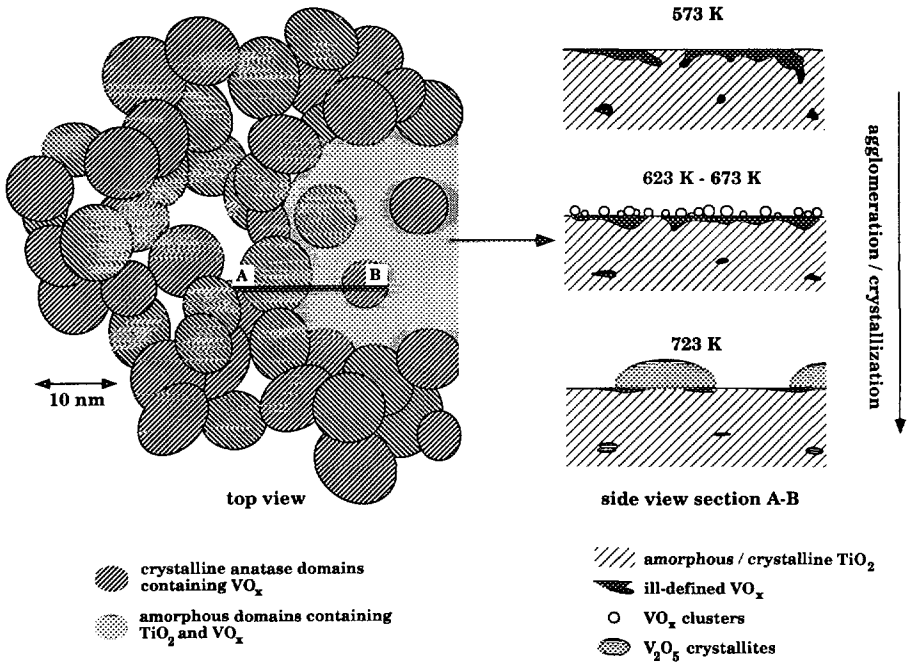


FIG. 11. Schematic representation of some structural features of vanadia–titania aerogels and of the changes induced by calcination at increasing temperatures (right diagram). The model is discussed in the text.

OH stretching region, where an increase in the V–OH infrared absorption bands is accompanied by a decrease in the signals due to acidic Ti–OH groups. In mineralogical terminology, one might summarize the changing influence of the vanadia on the structure of the aerogel as follows: For low contents, vanadia acts as a network modifier connecting titania domains. The vanadia is present in the form of mostly amorphous patches, including small defined vanadia clusters. With increasing vanadia content, amorphous vanadia layers cover and connect the titania domains, until at the highest contents, aggregation of the vanadia into three-dimensional crystallites becomes important.

The scanning electron micrographs (Fig. 6) can visualize this process, albeit on a micrometer scale. For the lower vanadia contents the morphology is similar to that of titania; with high vanadia loadings the surface resembles that of the vanadia aerogel.

The effects of a variation in the calcination temperature may be interpreted in terms of the schematic drawing shown in Fig. 11. At a '$V_2O_5$' content of 20 wt%, which was held constant for this series of experiments, the vanadia is present as amorphous species, of mostly ill-defined structure, after calcination under standard conditions (573 K). On an increase in the calcination temperature, the beginning of aggregation manifests as the appearance of oligomeric clusters in the Raman spectra. At the same time the vanadia starts to separate from the titania matrix and migrates to the surface. As a consequence, a larger fraction of $V_2O_n^+$ fragments is detected in the SIMS investigations. After calcination at 723 K, the segregated vanadia phase is present in crystalline form. The crystallization process is accompanied by a collapse of the aerogel surface area, as evidenced by the BET measurements (3).

At higher calcination temperatures, other authors [e.g., (6, 34)] have reported incorporation of vanadia into titania for catalysts prepared by conventional impregnation techniques. This phenomenon is intrinsically linked to the rutilization phenomenon. Saleh *et al.* (6) have argued that the mobility of *titania* is increased at higher temperatures, and that the latter forms rutile crystallites surrounding the previously formed crystalline $V_2O_5$ nuclei. In contrast, with our samples a significant growth of the *anatase* domains at higher calcination temperatures was detected by transmission electron microscopy (3), perhaps due to the fact that the vanadia is still well dispersed at this stage. Growth of the anatase crystallites is then expected to be accompanied by aggregation of the vanadia species on their surface.

The wet-chemical sol–gel temperature did not influence the reaction with the $TiO_2$ matrix. The chemical connection via the Ti–OH groups is similar for the range of temperatures investigated. However, with the highest sol–gel temperature studied (323 K), the observation of large numbers of small vanadia clusters points to enhanced cluster growth in the sol.

The structure of the catalysts was only slightly influ-

enced by the heating rate employed in the supercritical drying process. In accordance with the observations made when raising the sol–gel temperature, a large amount of small vanadia clusters appeared when the highest heating rate studied (120 K/h) was used.

The structure of the resulting catalyst does depend significantly on the vanadyl alkoxide precursor used. Replacement of the standard precursor, vanadyl tri-*n*-propoxide with the corresponding tri-isopropoxide results in an increased tendency toward vanadia agglomeration, which is already observed when standard preparation conditions are used. With respect to the state of vanadia agglomeration, the sample V20*ViP* (spectra not shown) is similar to V20*STA* catalysts calcined at 623 or 673 K and to the samples V20*SGT*323 or V20*HR*120, where high sol–gel temperatures or heating rates had been used. The steric hindrance introduced by the isopropoxy ligands of the vanadyl alkoxide precursor significantly lowers the hydrolysis rate (3), which is believed to influence the ratio of homo- to heterocondensation reactions.

## CONCLUSIONS

The first step in the preparation procedure, i.e., hydrolysis of tetrabutoxytitanium, results in the formation of small titania domains which persist on redispersion of the titania gel. Structural parameters of the dispersed vanadia show a pronounced dependence on the composition of the aerogels. At low vanadia contents, $VO_x$ centers are mainly tetrahedrally coordinated; they form small oligomeric clusters and amorphous patches on the surface of the titania domains. With higher vanadia concentrations, growth of the clusters is observed. Interaction with the titania matrix is strong, as evidenced by the absence of V=O stretching signals in the Raman spectra. Only for the highest investigated '$V_2O_5$' fraction of 30 wt% were both three-dimensional $V_2O_5$ paracrystallites and extended two-dimensional vanadia layers observed.

The sol–gel temperature does not have a major influence on the structure of the resulting aerogels. It appears that the anchoring reactions at the surface of the titania domains approach completion during the given reaction time at all temperatures investigated.

Calcination was found to be a critical parameter for the resulting structure and morphology of binary aerogels. When low calcination temperatures are used, vanadia forms amorphous overlayers of ill-defined structure, and is partly embedded in the titania matrix. Increasing migration of the vanadia to the surface is induced by calcination at higher temperatures. Agglomeration and crystallization of the vanadia represent the final stage of this thermally induced process. It leads finally to collapse of the aerogel surface. The SIMS results support the suggestion of a temperature-induced segregation of incorporated vanadia. The chemical interface, however, as reflected by the fraction of mixed vanadia–titania fragments, does not appear to be strongly influenced by calcination temperature.

A relatively high degree of dispersion of the vanadia–titania aerogels was deduced both from the SIMS and Raman spectroscopic results, despite the direct preparation procedure applied. This fact is most remarkable when compared with *supported* vanadia catalysts, on which highly aggregated $VO_x$ species and $V_2O_5$ crystallites are observed for loadings significantly exceeding the theoretical monolayer coverage. The excellent dispersion correlates well with the high activity of the V30 catalyst sample in the SCR reaction reported in our earlier study (3).

## ACKNOWLEDGMENTS

The authors are indebted to J. Kümmerlen and A. Sebald for recording the $^{51}V$ NMR spectra. Sincere thanks are due M. Kilo, G. Sauer, and M. Hund for their dedicated effort in obtaining the SIMS results. Financial support of this work by grants from the Deutsche Forschungsgemeinschaft (SFB 213), the Schweizerischer Nationaler Energieforschungsfonds (NEFF), and the Verband der Chemischen Industrie is gratefully acknowledged.

## REFERENCES

1. Brinker, C. J., and Scherer, G. W., "Sol–Gel Science." Academic Press, London/New York, 1990.
2. Schneider, M., and Baiker, A., *in* "Encyclopedia of Advanced Materials" (D. Bloor, R. J. Brook, M. C. Flemings, and S. Majahan, Eds.). Pergamon, Oxford, 1994.
3. Schneider, M., Maciejewski, M., Tschudin, S., Wokaun, A., and Baiker, A., *J. Catal.* **149,** (1994).
4. Cristiani, C., Forzatti, P., and Busca, G., *J. Catal.* **116,** 586 (1989).
5. Schraml, M., Fluhr, W., Wokaun, A., and Baiker, A., *Ber. Bunsenges. Phys. Chem.* **93,** 852 (1989).
6. Saleh, R. Y., Wachs, I. E., Chan, S. S., and Chersich, C. C., *J. Catal.* **98,** 102 (1986).
7. Saleh, R. Y., and Wachs, I. E., *Appl. Catal.* **31,** 87 (1987).
8. Bond, G. C., *J. Catal.* **116,** 531 (1989); Bond, G. C., and Tahir, S. F., *Appl. Catal.* **71,** 1 (1991).
9. Went, G., Leu, L. J., and Bell, A. T., *J. Catal.* **134,** 479 (1992); Went, G., Leu, L. J., Rosin, R. R., and Bell, A. T., *J. Catal.* **134,** 492 (1992).
10. Schraml-Marth, M., Wokaun, A., Pohl, M., and Krauss, H. L., *J. Chem. Soc. Faraday Trans. I* **87,** 2635 (1991).
11. Scharf, U., Schraml-Marth, M., Wokaun, A., and Baiker, A., *J. Chem. Soc. Faraday Trans. I* **87,** 587 (1991).
12. Handy, B., Baiker, A., Schraml-Marth, M., and Wokaun, A., *J. Catal.* **133,** 1 (1992).
13. Le Costumer, L. R., Taouk, B., Le Meur, J., Payen, E., Guelton, M., and Grimblot, J., *J. Phys. Chem.* **92,** 1230 (1988).
14. Eckert, H., and Wachs, I. E., *J. Chem. Phys.* **93,** 6796 (1989).
15. Sobalik, Z., Markvart, M., Stopka, P., Lapina, O. B., and Mastikhin, V. M., *J. Mol. Catal.* **71,** 69 (1992).
16. Walther, K. L., Kümmerlen, J., Wokaun, A., and Baiker, A., *Ber. Bunsenges. Phys. Chem.* **97,** 772 (1993).
17. Meier, M., Carron, K. T., Fluhr, W., and Wokaun, A., *Appl. Spectrosc.* **17,** 4 (1986).

18. Schild, Ch., Wokaun, A., and Baiker, A., *Surf.Sci.* **269/270,** 520 (1992).
19. Van Veen, J. A. R., Veltmaat, F. T. G., and Jonkers, G., *J. Chem. Soc. Chem. Commun.*, 1656 (1985).
20. Topsoe, N.-Y., *J. Catal.* **128,** 499 (1991).
21. Rajadhyaksha, R. A., and Knözinger, H., *Appl. Catal.* **51,** 81 (1991).
22. Busca, G., and Lavelley, J. C., *Specrochim. Acta A* **42,** 443 (1986).
23. Schraml-Marth, M., Wokaun, A., and Baiker, A., *J. Catal.* **124,** 86 (1990), and references therein.
24. Ono, T., Mukai, T., Miyata, H., Ohno, T., and Hatayama, F., *Appl. Catal.* **49,** 273 (1989).
25. Eckert, H., Deo, G., Wachs, I. E., and Hirt, A. M., *Colloids Surf.* **45,** 347 (1990).
26. Gilson, T. R., Bisri, O. F., and Cheetham, N., *J. Chem. Soc. Dalton Trans.*, 291 (1973).
27. Griffith, W. P., and Wickins, T. D., *J. Chem. Soc. (A)*, 1088 (1966).
28. Beattie, I. R., and Gilson, T. R., *J. Chem. Soc. (A)*, 2322 (1969).
29. Machej, T., Haber, J., Turek, A. M., and Wachs, I. E., *Appl. Catal.* **70,** 115 (1991).
30. Handy, B. E., Gorzkowska, I., Nickl, J., Baiker, A., Schraml-Marth, M., and Wokaun, A., *Ber. Bunsenges. Phys. Chem.* **96,** 1832 (1992).
31. Sanchez, C., Livage, J., and Luccazeau, G., *J. Raman Spectrosc.* **12,** 68 (1982).
32. Kijenski, J., Baiker, A., Glinski, M., Dollenmeier, P., and Wokaun, A., *J. Catal.* **101,** 1 (1986).
33. Wokaun, A., Schraml, M., and Baiker, A., *J. Catal.* **116,** 595 (1989).
34. Kozlowski, R., Pettifer, R. F., and Thomas, J. M., *J. Phys. Chem.* **87,** 5176 (1983).